AGU PUBLICATIONS

JGR

Journal of Geophysical Research: Space Physics

RESEARCH ARTICLE

10.1002/2016JA023659

Key Points:

- TIDs induced by gravity waves generated by the Tohoku tsunami traveled over long distances above the West Coast of the U.S.
- After the forcing stopped at the shore, TIDs continued to propagate inland and gradually decayed
- Reverse ray tracing to show that the Tohoku tsunami was likely the source of these TIDs

Supporting Information:

- Supporting Information S1
- Movie S1
- Movie S2

Correspondence to:

I. Azeem,
iazeem@astraspace.net

Citation:

Azeem, I., S. L. Vadas, G. Crowley, and J. J. Makela (2017), Traveling ionospheric disturbances over the United States induced by gravity waves from the 2011 Tohoku tsunami and comparison with gravity wave dissipative theory, *J. Geophys. Res. Space Physics*, *122*, doi:10.1002/2016JA023659.

Received 8 NOV 2016
Accepted 8 FEB 2017
Accepted article online 13 FEB 2017

Traveling ionospheric disturbances over the United States induced by gravity waves from the 2011 Tohoku tsunami and comparison with gravity wave dissipative theory

Irfan Azeem[1], Sharon L. Vadas[2], Geoff Crowley[1], and Jonathan J. Makela[3]

[1]ASTRA LLC, Boulder, Colorado, USA, [2]NorthWest Research Associates, Boulder, Colorado, USA, [3]Department of Electrical and Computer Engineering, University of Illinois at Urbana-Champaign, Urbana, Illinois, USA

Abstract The 11 March 2011 Tohoku earthquake generated a massive tsunami off the Pacific coast of Japan, which launched intense atmospheric gravity waves (AGWs) in the atmosphere. Within the context of this study, the Tohoku tsunami event was unique in the sense that it enabled a rare, controlled experiment for investigating how AGWs are launched, propagate, and dissipate in relation to tsunamis. This tsunami was a long-lived, rapidly traveling source of a rich spectra of AGWs excited just above the ocean-atmosphere interface. In this paper we use GPS total electron content (TEC) data from the United States (U.S.) to look for these AGWs in the ionosphere via their signatures as traveling ionospheric disturbances (TIDs). We find a spectrum of TIDs in the TEC data propagating in the direction of the tsunami that last for several hours over the West Coast of the U.S. and as far inland as western Colorado. The observed TIDs have periods that range from 14 to 30 min, horizontal wavelengths that range from 150 and 400 km, and horizontal phase speeds that range from 180 to 260 m/s. We use reverse ray tracing to show that the Tohoku tsunami was likely the source of these TIDs. Using the networks of GPS receivers in the U.S., we map the tsunami-launched TIDs over the western U.S. and investigate the spectrum of gravity waves enabling an enhanced understanding/verification of the properties of AGWs as a function of the launch angle.

1. Introduction

Atmospheric gravity waves (AGWs) are created by perturbations in the stable atmosphere, with gravity being the restoring force [*Hines*, 1960; *Yeh and Liu*, 1974; *Francis*, 1975]. As AGWs propagate from their source region into the thermosphere, they create periodic oscillations in the ionospheric electron density via ion-neutral collisions [*Hooke*, 1968; *Bowman*, 1990; *Hocke and Schlegel*, 1996] until they dissipate from molecular viscosity, ion drag, and other processes [*Richmond*, 1978; *Hickey and Cole*, 1988; *Vadas and Fritts*, 2005; *Heale et al.*, 2014]. These oscillations in the ionosphere are called traveling ionospheric disturbances (TIDs). Such TIDs are not self-supporting waves; meaning that they cannot exist and propagate on their own without the underlying AGWs. However, because they “follow” the AGWs and may be easier to detect, they can provide excellent tools by which to detect and quantify the propagation and dissipation of AGWs excited by lower atmosphere sources.

There are many mechanisms that can create AGWs. AGWs can be generated in auroral regions from Joule heating caused by geomagnetic storms [e.g., *Richmond*, 1978; *Hunsucker*, 1982; *Rice et al.*, 1988]. Severe meteorological events such as thunderstorms and tornadoes also generate AGWs; these AGWs can appear as concentric rings at higher altitudes if the intervening neutral winds are small [*Dewan et al.*, 1998; *Taylor and Hapgood*, 1988; *Tsunoda*, 2010; *Sentman et al.*, 2003; *Suzuki et al.*, 2007; *Yue et al.*, 2009; *Vadas et al.*, 2009, 2012; *Suzuki et al.*, 2013]. The signatures of concentric AGWs have also been observed in the ionosphere [*Nishioka et al.*, 2013; *Azeem et al.*, 2015] Several studies have suggested that deep convection in the troposphere [*Fovell et al.*, 1992; *Alexander et al.*, 1995; *Lane et al.*, 2001] is one of the primary drivers of AGWs that can propagate upward into the mesopause region [*Alexander*, 1996; *Holton and Alexander*, 1999; *Walterscheid et al.*, 2001; *Vadas and Fritts*, 2009; *Vadas et al.*, 2009, 2012]. Recent theoretical studies have shown that some AGWs from deep convection can also propagate efficiently into the thermosphere [*Vadas*, 2007; *Kherani et al.*, 2009; *Paulino et al.*, 2012; *Vadas and Liu*, 2009, 2013; *Vadas and Crowley*, 2010; *Vadas et al.*, 2014]. AGWs can also be man-made; nuclear detonations have been shown to launch AGWs into Earth’s atmosphere [*Hines*, 1967; *Row*, 1967]. Other natural disasters can also generate AGWs, including earthquakes [*Hasbi et al.*, 2011, and references therein] and tsunamis [*Artru et al.*, 2005; *Liu et al.*, 2006; *Lognonńe et al.*, 2006; *Rolland et al.*, 2010;

Hickey et al., 2010; *Makela et al.*, 2011; *Matsumura et al.*, 2011; *Galvan et al.*, 2011, 2012; *Hickey et al.*, 2010; *Occhipinti et al.*, 2006, 2008a, 2011, 2013; *Garcia et al.*, 2014; *Broutman et al.*, 2014; *Vadas et al.*, 2015].

AGWs at ionospheric heights have been inferred from their TID signatures using either optical or radio remote sensing techniques. All-Sky Imagers (ASIs) that detect the 630.0 nm "red line" airglow emission from atomic oxygen resulting from the dissociative recombination of O_2^+ can produce nighttime images of horizontal 2-D structures in the ionosphere/thermosphere system [*Makela and Otsuka*, 2011, and references therein] including the impression of AGWs in the thermosphere [*Taylor et al.*, 1998; *Fukushima et al.*, 2012; *Smith et al.*, 2013; *Paulino et al.*, 2016]. These ASI images can provide insights into the 2-D wave properties and morphology of ionospheric structures during the nighttime, allowing for the study of their spatiotemporal properties [*Garcia et al.*, 2000; *Kelley et al.*, 2000; *Duly et al.*, 2013].

Radio techniques such as HF sounding can also be used to record TIDs propagating in the ionosphere [*Crowley and McCrea*, 1988; *Williams et al.*, 1988; *Crowley and Rodrigues*, 2012]. Recently, it has been shown that modern incoherent scatter radars can measure the 3-D structure of TIDs [*Nicolls and Heinselman*, 2007; *Vadas and Nicolls*, 2009; *Nicolls et al.*, 2010, 2014]. An emerging technique is to use total electron content (TEC) information from a dense network of dual-frequency GPS receivers to form 2-D spatial maps of TIDs [e.g., *Tsugawa et al.*, 2007; *Astafyeva et al.*, 2011; *Nishioka et al.*, 2013] at all local times. We note here that a TID is discernible in the TEC data from ground-based GPS receivers only if the vertical wavelength of the underlying AGW is much larger than the thickness of the *F* layer or if the AGW consists of mostly one phase along the integrated path; either of these situations will ensure that the integrated electron density amplitude is not reduced too much from cancelations. This latter possibility may occur if the AGW has a large amplitude within the *F* layer but then rapidly dissipates or if the line of sight of a slant TEC is oriented along a constant phase line of an AGW.

Historically, TIDs have been classified as medium scale or large scale [e.g., *Crowley et al.*, 1987; *Hocke and Schlegel*, 1996; *Crowley and Rodrigues*, 2012]. Medium-scale TIDs (MSTIDs) tend to have wave periods in the 10–50 min range and propagate with horizontal phase speeds less than 300 m/s. In contrast, large-scale TIDs have periods larger than 30 min and propagate with phase speeds exceeding ~300 m/s. For many years, these medium-scale waves were thought to originate exclusively in the lower atmosphere. This idea has recently been challenged as evidence has emerged that some medium-scale waves may be secondary AGWs generated in the thermosphere via a two-step coupling process [*Vadas and Crowley*, 2010]; in this process, the primary convectively generated AGWs dissipate from molecular viscosity in the thermosphere, thereby depositing momentum and energy. This deposition excites secondary AGWs having phase speeds $>$100 m/s. Additionally, the large-scale waves were previously thought to originate exclusively in the auroral regions from geomagnetic activity. This idea has also been challenged because theoretical studies have shown that this same two-step coupling process also generates large-scale secondary AGWs in the thermosphere [*Vadas and Liu*, 2009, 2013; *Vadas et al.*, 2014]. Furthermore, several studies have suggested that there is another class of TIDs which can occur at middle and low latitudes during the nighttime. These nighttime TIDs, exhibiting bands of wave-like features in electron density aligned along NW-SE in the Northern Hemisphere (NE-SW in the Southern Hemisphere), are thought to be caused by electro-buoyancy waves [*Miller et al.*, 1997; *Saito et al.*, 2011; *Otsuka et al.*, 2004]. Their source is commonly attributed to the Perkins instability [*Kelley and Fukao*, 1991; *Miller et al.*, 1997; *Kelley and Miller*, 1997; *Duly et al.*, 2014]. Unfortunately, they have also been labeled as "MSTIDs" which has caused considerable confusion in the literature. The focus of the present study is on "classical" MSTIDs that are associated with the collisional coupling between the ionosphere and AGWs.

The 11 March 2011 Tohoku earthquake and subsequent tsunami-launched AGWs which were observed over long distances across the Pacific Ocean basin [e.g., *Makela et al.*, 2011]. The signatures of the AGWs generated by both the earthquake and tsunami have been the subject of extensive study, with GPS-derived TEC providing a wealth of information on the different types of TIDs that were generated [e.g., *Tsugawa et al.*, 2011; *Astafyeva et al.*, 2011; *Liu et al.*, 2011; *Rolland et al.*, 2011; *Galvan et al.*, 2012]. These studies have investigated various components of the AGWs in the ionosphere close to the epicenter of the earthquake. Near the Tohoku earthquake epicenter, TIDs were observed propagating away from the epicenter with phase speeds generally attributed to acoustic, Rayleigh, and AGWs [*Galvan et al.*, 2012]. Some of these TIDs were associated with the seismic source itself rather than that of the tsunami [*Rolland et al.*, 2011]. The ionospheric signatures of the tsunami-generated AGWs were also observed for the first time in the 630 nm airglow using an imager located in Maui, Hawaii [*Makela et al*., 2011], and later over South America [*Smith et al*., 2015]. The airglow images of nighttime TIDs over Hawaii [*Makela et al*., 2011] showed two distinct wave features: (a) long-period ($T = 26.2 \pm 3.1$ min) and (b) short-period (14.2 ± 2.7 min) waves traveling away from the earthquake epicenter with phase speeds of 184.5 ± 33.8 m/s and 222.9 ± 52.4 m/s, respectively. These AGWs were likely created by the tsunami. Recently, *Meng et al*. [2015] expanded the observational domain by examining the tsunami-generated TIDs over the West Coast of the U.S. In contrast to the present study, *Meng et al*. [2015] considered a single period of the AGW wave packet in characterizing the TIDs and was limited to only 16 GPS TEC measurements. *Crowley et al*. [2016] presented maps of TIDs over the U.S. but focused only on the two largest components within the wave packet. As we will show in this paper, the Tohoku tsunami was composed of an entire wave packet that continuously launched spectra of AGWs which propagated into the thermosphere and ionosphere. This study, for the first time, looks at the full spectrum of the wave packet in the ionosphere over the West Coast of the U.S. and uses the results to demonstrate that the TID observations are consistent with AGW theory.

In this work, we use GPS receivers distributed throughout the continental United States (CONUS) to observe TIDs associated with the 11 March 2011 Tohoku earthquake at a significantly greater distance from the epicenter than has previously been reported. We use 2-D spatial maps of GPS TEC perturbations to calculate TID parameters, including horizontal wavelengths, phase speeds, and periods. The results presented herein provide a detailed view of the evolution of the AGW spectrum at ionospheric heights. From a theoretical perspective, it is well understood that the AGW spectrum and characteristics undergo some level of modification as the wave packet propagates vertically (and horizontally) into the atmosphere due to variations of the background wind and temperature. The intense TIDs generated by the Tohoku tsunami present a unique opportunity for providing observational evidence with which to test various aspects of AGW theory such as wave generation, wave propagation, wave dissipation, and the resulting evolution of the spectral shape of the wave packet. This paper reveals the following: (1) the presence of TIDs generated by the Tohoku tsunami on the West Coast of the U.S.; (2) the propagation of these TIDs far inland, where the underlying tsunami source is no longer present; and (3) the progressive modification of the spectral composition of the wave packet as it propagates away from the source region into the thermosphere and undergoes viscous dissipation. The TID data and associated analyses present a detailed look at the propagation regime of the TIDs over the CONUS and provide an observational verification of AGW dissipative theory.

2. GPS TEC Data

The TID images presented in this paper were created by combining GPS TEC data from over 4000 sites in the U.S. Our approach for generating these TID images is as follows. First, we compute slant TEC values along oblique raypaths to each PRN which are then converted to vertical TEC (VTEC) at subionospheric pierce points (IPPs) using the obliquity factor model described by *Kaplan and Hagerty* [2006]. The effective altitude of the IPP over the CONUS region is assumed to be equal to the height of the F_2 peak (or h_mF_2) predicted by the International Reference Ionosphere (IRI) model [*Bilitza et al*., 2014]. Figure 1 shows several IRI electron density profiles between 16 and 18 UT on 11 March 2011 over Mineral, CA (40.22°N, 121.43°W). These IRI profiles are representative of the ionospheric conditions over the western U.S. where TIDs were observed. The F_2 layer peak occurs at $z = 250$ km. We then compute perturbations in TEC by detrending VTEC using a 40 min running mean for each PRN followed by $0.15° \times 0.15°$ binning in latitude and longitude and horizontal smoothing of the resulting TEC map using a 2-D Gaussian filter with a full width at half maximum of 0.75° in both dimensions. Our TEC analysis scheme is similar to that of *Tsugawa et al*. [2007] and *Nishioka et al*. [2013], with the exception that we compute VTEC prior to detrending.

3. Three-Dimensional Reverse Ray Trace Model

Our 3-D ray trace model incorporates an anelastic AGW dispersion relation which includes realistic dissipation in the thermosphere from kinematic viscosity and thermal diffusivity [*Vadas and Fritts*, 2005; *Vadas*, 2007]. This dispersion relation is valid for AGWs with periods less than an hour during the daytime and a few hours during the nighttime when ion drag can be neglected [*Gossard and Hooke*, 1975]. This dispersion relation also neglects wave-induced diffusion and the Coriolis force. The former is likely not important for AGWs with

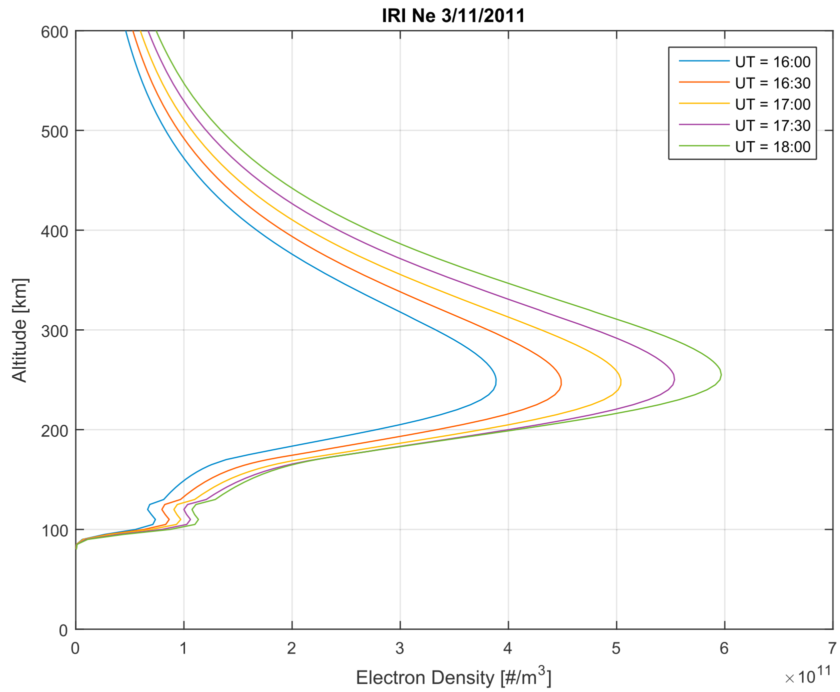

Figure 1. Electron density profiles over Mineral, CA (40.22°N, 121.431°W) from the IRI model on 11 March 2011 from 16 to 18 UT.

periods less than an hour [*Del Genio et al.*, 1979], and the latter is not important for AGWs with periods less than a few hours. Because the AGWs observed here (in the TEC) have periods less than an hour, we are justified to neglect ion drag, wave-induced diffusion, and the Coriolis force.

Our ray trace model can be utilized in the forward and/or reverse modes [e.g., *Vadas and Crowley*, 2010]. This ray trace model includes horizontally, vertically, and temporally varying background winds and temperatures, dissipative filtering, critical level filtering, evanescence, and frequency changes from time-varying background winds. In this study, we use a combined data set from the European Centre for Medium-Range Weather Forecasting (ECMWF) model and thermosphere-ionosphere-mesosphere electrodynamics general circulation model (TIMEGCM) for the background neutral temperature and wind and utilize empirical, analytical formulas to determine the molecular mass and heat capacity ratio (γ) from the background density [*Vadas*, 2007, equations (3) and (4)].

4. Observational Results

On 11 March 2011 at 05:46:23 universal time (UT) a magnitude 9.0 earthquake occurred near the northeast coast of Honshu, Japan. The earthquake produced a huge tsunami with 9 m waves that caused widespread destruction along the coast of the northern part of Japan [*Fujii et al.*, 2011]. Over the ensuing hours, the tsunami waves traveled across the Pacific basin to Alaska and down the Pacific coast of North and South America [*Tang et al.*, 2012]. In the aftermath of the Tohoku earthquake, tsunami warnings were issued in many countries bordering the Pacific [*Fraser et al.*, 2012; *Suppasri et al.*, 2013]. The first-arrival tsunami traveltimes (TTTs) are shown in Figure 2 (http://nctr.pmel.noaa.gov/honshu20110311/). The time in UT at any given location/time is then computed by adding the TTT to 05:46:23 UT. The TTT map in Figure 2 shows that the tsunami wave reached the West Coast of the United States about 10 to 12 h after the earthquake struck Japan. As the tsunami wavefronts reached the West Coast of the U.S., they were oriented at an angle of ~30° east of north, consistent with the tsunami propagation azimuth of ~120° (measured clockwise from north).

Figure 3 compares the VTEC perturbations measured on 11 March 2011 (solid line) with those from the previous day (dashed line) from a Continuously Operating Reference Station (CORS) receiver in Mineral, CA. This

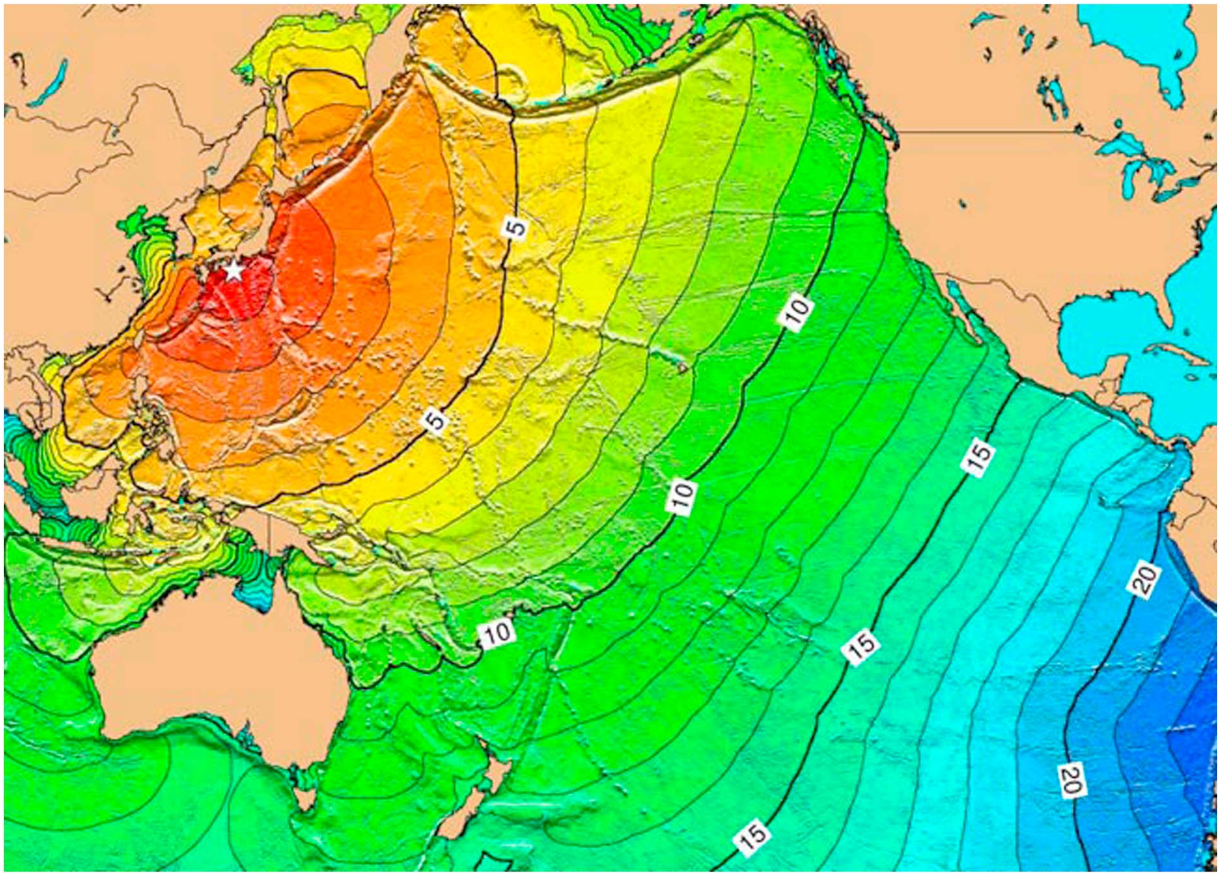

Figure 2. NOAA National Geophysical Data Center's map of tsunami arrival time (in hours) during the 2011 Japan tsunami (http://www.ngdc.noaa.gov/hazard/11mar2011.html) [after *Crowley et al*., 2016].

is the same location as used in Figure 1. Figure 3a shows the band-pass filtered VTEC data from the satellite pass of PRN 21 between 15 and 20 UT, while Figure 3b shows the corresponding satellite elevation as a function of UT. The data on 11 March 2011 show a large sinusoidal variation around 16:30 UT, about 11 h after the Tohoku earthquake in Japan. The amplitude of the VTEC perturbation was about ±1.1 total electron content unit (TECU, 1 TECU = 10^{16} el m^{-2}) at 17:30 UT (1 TECU = 1×10^{16} #/m^2). TEC variations at low-elevation angles are likely to be affected by multipath. However, Figure 3 shows that during much of the time the elevation of the GPS satellite SVN 21 was well above 40° suggesting that the observed VTEC variations were not caused by low-elevation effects and multipath but rather by geophysical variations in the ionosphere. Similar perturbations were also seen on other receiver-satellite links for receivers distributed across the CONUS, confirming that the TEC perturbations shown in this figure were widespread. In contrast, the amplitude of the VTEC perturbations on 10 March 2011 was approximately ±0.05 TECU, close to the noise floor of most dual-frequency GPS receivers.

Figure 4 shows the evolution of the TIDs over the CONUS after the initial tsunami event. The figure shows four snapshots of the TID map between 15:30 and 19:15 UT to illustrate the spatial extent, geometry, and propagation of the TIDs. We note here that the images in the figure have been saturated by limiting the gray scale to ±0.03 TECU. This saturation allows the TID structures to be visually overemphasized in the images. At first glance, the scales of the TEC perturbations in the maps could mistakenly be assumed to be on the order of 0.03 TECU. However, the TID amplitudes are much larger than suggested by the choice of the scale in Figure 4. In fact, the amplitude of the TID in the unsmoothed TEC data is ±1.1 TECU with a measurement uncertainty of 0.02 TECU (see Figure 3). At 15:30 UTC (Figure 4, top left), the entire domain is devoid of any coherent wave structure. At 16:45 UTC (Figure 4, top right), planar waves are present throughout the Pacific coast region, with lines of constant phase oriented parallel to the northeastward to southwestward direction. Note that the orientation of the TID constant phase lines is similar to the angle of the tsunami

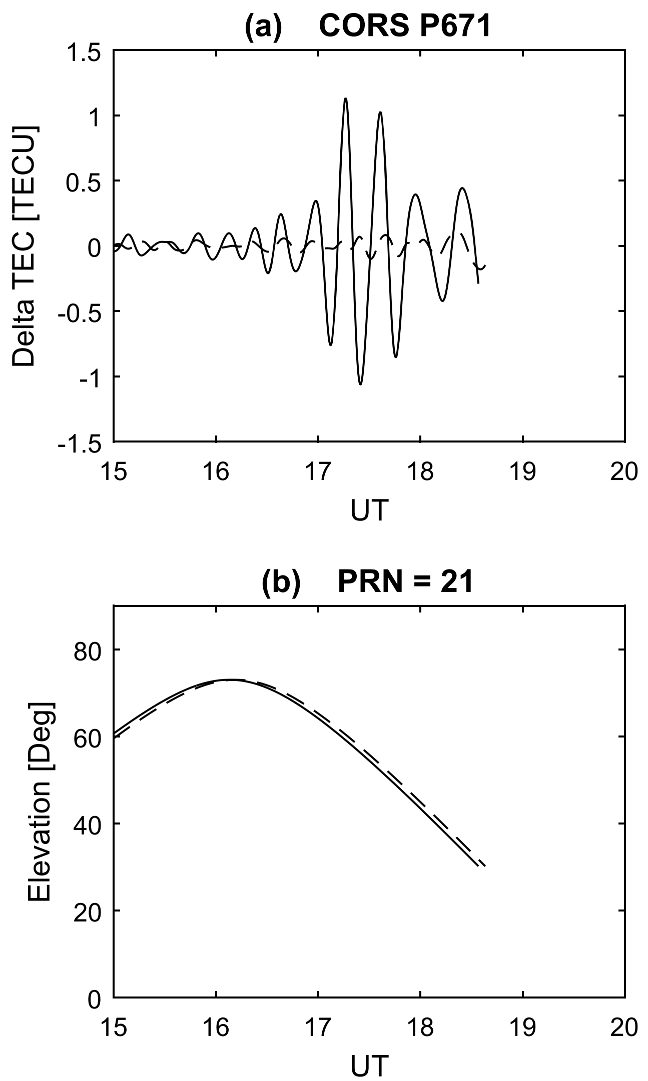

Figure 3. (a) VTEC perturbations seen on a GPS receiver located in Oregon at 44.97°N latitude, 122.95°W longitude and (b) the elevation angle of the GPS satellite SVN 15 on 10 March 2011 (dashed lines) and 11 March 2011 (solid lines). Large sinusoidal variations in VTEC are seen around 16:30 UT on 11 March 2011. In contrast, no such large variations in VTEC are seen on 10 March 2011.

phase fronts near the West Coast of the U.S. (see Figure 2). This similarity in phase fronts of the observed TIDs and the tsunami is likely indicative of the causal relationship between the two. This will be further discussed within the context of AGW theory in section 6. Similar TID structures are also present in the TEC map 30 min later, at 17:00 UT (Figure 4, bottom left). An animation of the TEC perturbation map (included as Movie S1) at a cadence of 1 min shows that these TIDs propagate as a wave packet toward the southeast and have an average azimuth of 121.8° (measured clockwise from north). The azimuth is in good agreement with the propagation direction of the tsunami near the U.S. West Coast. In total, these TIDs persisted for about 4 h after they were first seen in the GPS TEC measurements at 15:46 UT, although most of the TID activity occurs prior to 18:15 UT (which is a total of ~2.5 h) and the peak of the activity occurred from 16:30 to 17:30 UT. By 19:15 UT (Figure 4, bottom right), the TIDs are mostly absent in the data.

To contrast these TIDs from a quiescent interval, we also show an animation (see Movie S2) of the TEC perturbations on 10 March 2011 for the same 15–20 UT duration as shown in Movie S1. While TEC structures are also present over the CONUS on 10 March 2011, the TIDs seen on the West Coast on 10 March 2011 are much weaker, more localized, and shorter lived than the tsunami-generated TIDs on 11 March 2011. In contrast, the TIDs observed on 11 March 2011 have large amplitudes and, more importantly, the timing of their appearance over the West Coast of the U.S. and their morphology suggest a striking association with the Tohoku tsunami as it approached the U.S. coastline. The differences in the TIDs on the western part of the U.S. on these two days suggest different source mechanisms.

Wave features are also visible east of Texas at 19:15 UT on 11 March 2011 (Figure 4, bottom right). They propagate slightly more southward than the TIDs over the West Coast of the U.S. Using only the data shown in Figure 4 (bottom right), we cannot determine if the TIDs east of Texas are an eastward extension of the waves seen on the West Coast or are generated by a different source (e.g., deep convection in the troposphere). However, when combined with the fact that similar wave features are also seen the previous day, it is likely that the eastward moving TIDs east of Texas on 11 March 2011 are not associated with the tsunami wave; they might have been created by a weather front or some other source. In this paper we do not investigate the TIDs east of Texas. The rest of the paper will focus on the TIDs that extend from the west cost of the U.S. to Colorado. Note that the TIDs in Figure 4 (top right and bottom left) exhibit a sharp cutoff at ~102°W at the

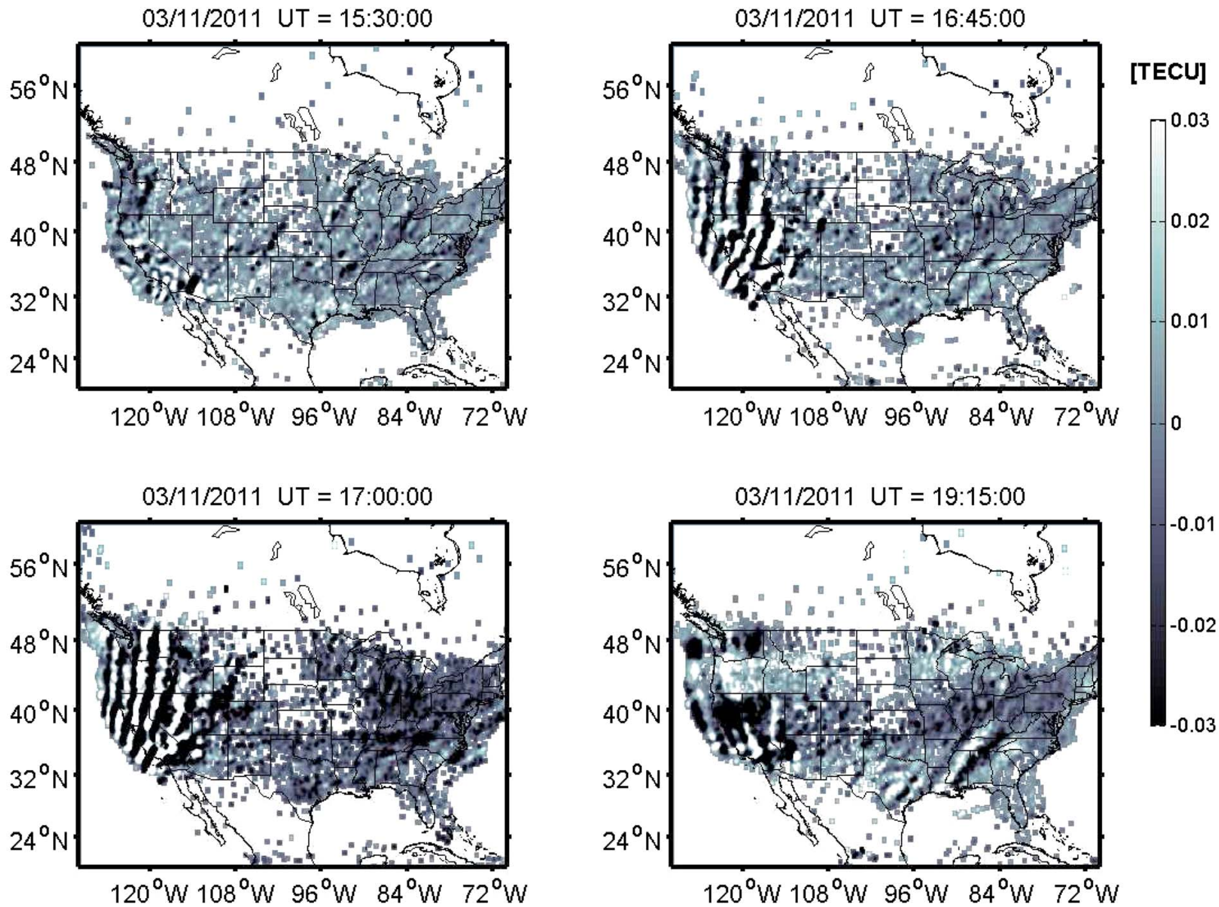

Figure 4. Two-dimensional maps of TEC perturbations at (top left) 15:30 UT, (top left) 16:45 UT, (bottom left) 17:00 UT, and (bottom right) 19:15 UT. These maps show planar TID wavefronts over the West Coast of the United States.

northern edge of the wave packet and ~114°W at the southern edge. This occurs because of dissipative filtering of the AGWs from molecular viscosity in the thermosphere, as is discussed in detail in section 6.

A wavelet analysis of the observed TIDs reveals how the wave periods within the gravity wave packet change with longitude from the West Coast of the U.S. through Colorado and Wyoming. Figure 5 shows the normalized power as a function of period and longitude for six different geographic latitudes (LAT). In all cases, the TIDs have shorter periods near the western edge of the U.S. at 125°W ($\tau \sim 10$–15 min) and have longer periods toward the eastern edge of the TID wave packet at 115°W ($\tau \sim 18$–25 min). The figure also shows that the wave period increases approximately linearly with longitude. If the source is near the western part of the U.S., this illustrates the dispersive nature of a spectrum of GWs with differing periods since the propagation angle that an AGW makes with the horizontal (ξ) is directly dependent on the intrinsic period of the AGW (τ_{Ir}): $\tau_{Ir} = \tau_B / \sin(\xi)$, where τ_B is the buoyancy period and we have assumed weak winds [e.g., *Vadas et al.*, 2009, equation (19)]. Thus, shorter-period waves propagate more vertically than longer-period waves. Therefore, an initial wave packet with a mix of different periods will gradually disperse horizontally as the shorter-period waves reach the ionosphere closer horizontally to the source than the longer-period waves. The AGWs reaching the *F* region over Washington/Oregon/California would have had a steeper ascent angle (therefore smaller intrinsic periods and shorter horizontal distance traveled), while those AGWs reaching the *F* region over Utah and western Colorado and Wyoming would have had a smaller angle from the horizontal (therefore larger intrinsic periods and longer horizontal distance traveled).

The preceding argument is based on the background wind being similar along the different AGW raypaths. In Figure 4 (top right), we see that the eastern and western edges of the TIDs are separated by ~12° in longitude. Because the background winds are mainly caused by tides and planetary waves which have longitudinal variation over ~20° or more, the AGWs causing the TEC perturbations are likely to have passed through

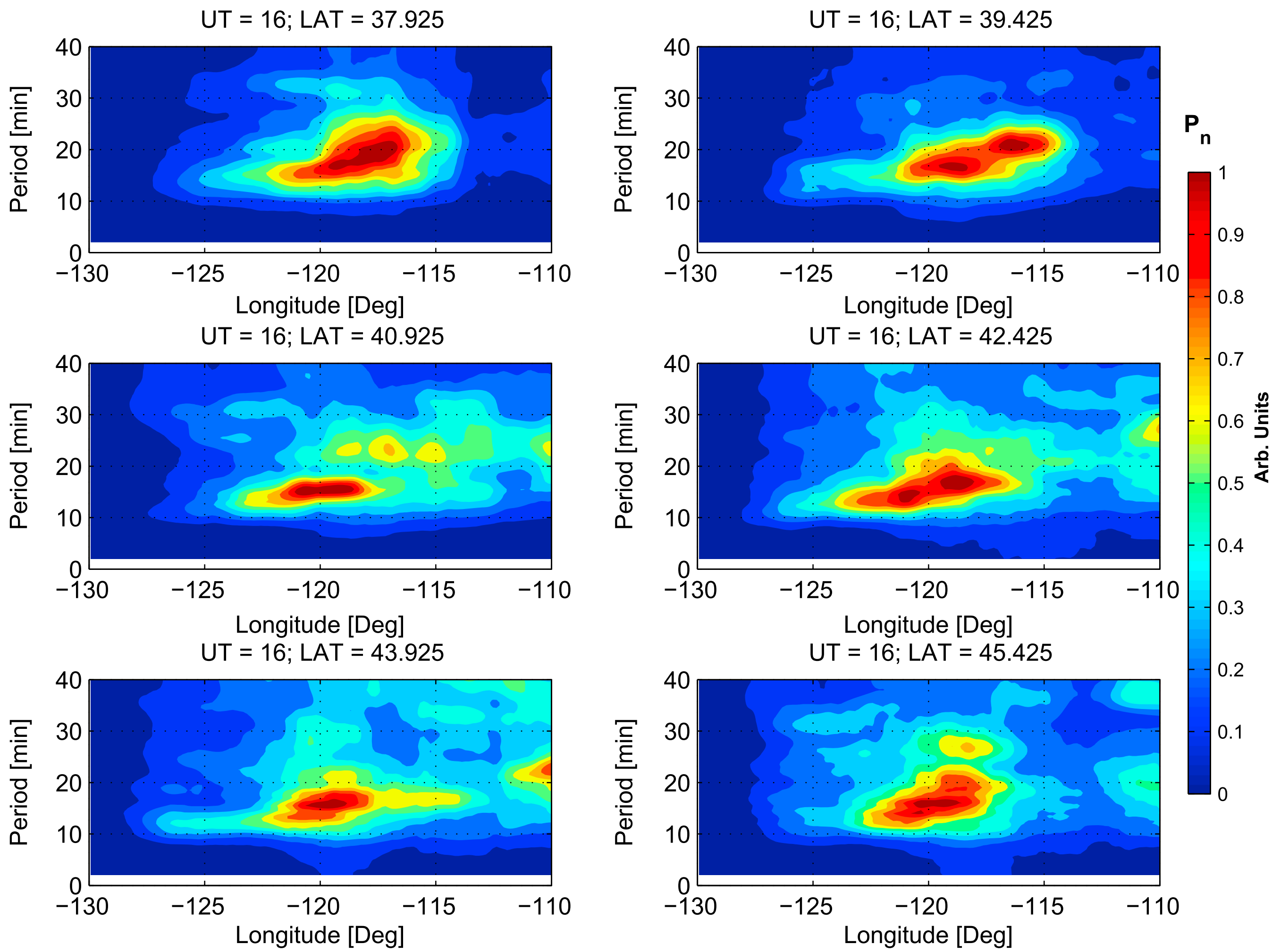

Figure 5. Normalized wavelet spectrogram of the TID period as a function of longitude for various latitudes.

similar background winds. Our model simulations using the TIMEGCM also show this near uniformity in the background horizontal winds up to and including the *F* region over the western U.S. Therefore, it is unlikely that the spread in the AGW locations at $z = 250$ km is due to the variation in the background wind. Additionally, we are unaware of any other source that could have created the AGWs seen extending from the West Coast of the U.S. to Colorado/Wyoming with phase lines oriented north-south over thousands of kilometers. (The only other possible source might be terminator-generated AGWs. However, these AGWs have very large horizontal wavelengths of thousands of kilometers [*Forbes et al.*, 2008; *Liu et al.*, 2009].) It is well known that the angle an AGW makes with the horizontal is directly related to its period, with the larger-period AGWs propagating more horizontally and the shorter-period AGWs propagating more vertically. Therefore, the most likely reason for the shift in the observed period with longitude is a tsunami-generated spectrum AGWs having a range of periods.

The dispersion of AGWs in the ionosphere is also illustrated in Figure 6, which shows the normalized wavelet spectrum of the horizontal wavelength as a function of longitude for the same set of latitudes as shown in Figure 5. The horizontal wavelengths (λ_H) of the TIDs are ~150–250 km at the western edge of the U.S. (125°W) and are ~250–400 km at the eastern edge of the TIDs (115°W). Thus, the horizontal wavelength increases with longitude in an approximately linear manner. The results in Figures 5 and 6 are consistent with our theoretical understanding of the propagation and dissipation of AGWs in the thermosphere (employing the dissipative AGW dispersion relation). To explain the increase of TID horizontal wavelength from λ_H ~150–250 km at the western edge of the U.S. to λ_H ~250–400 km at 115°W, we examine the purple dashed line for

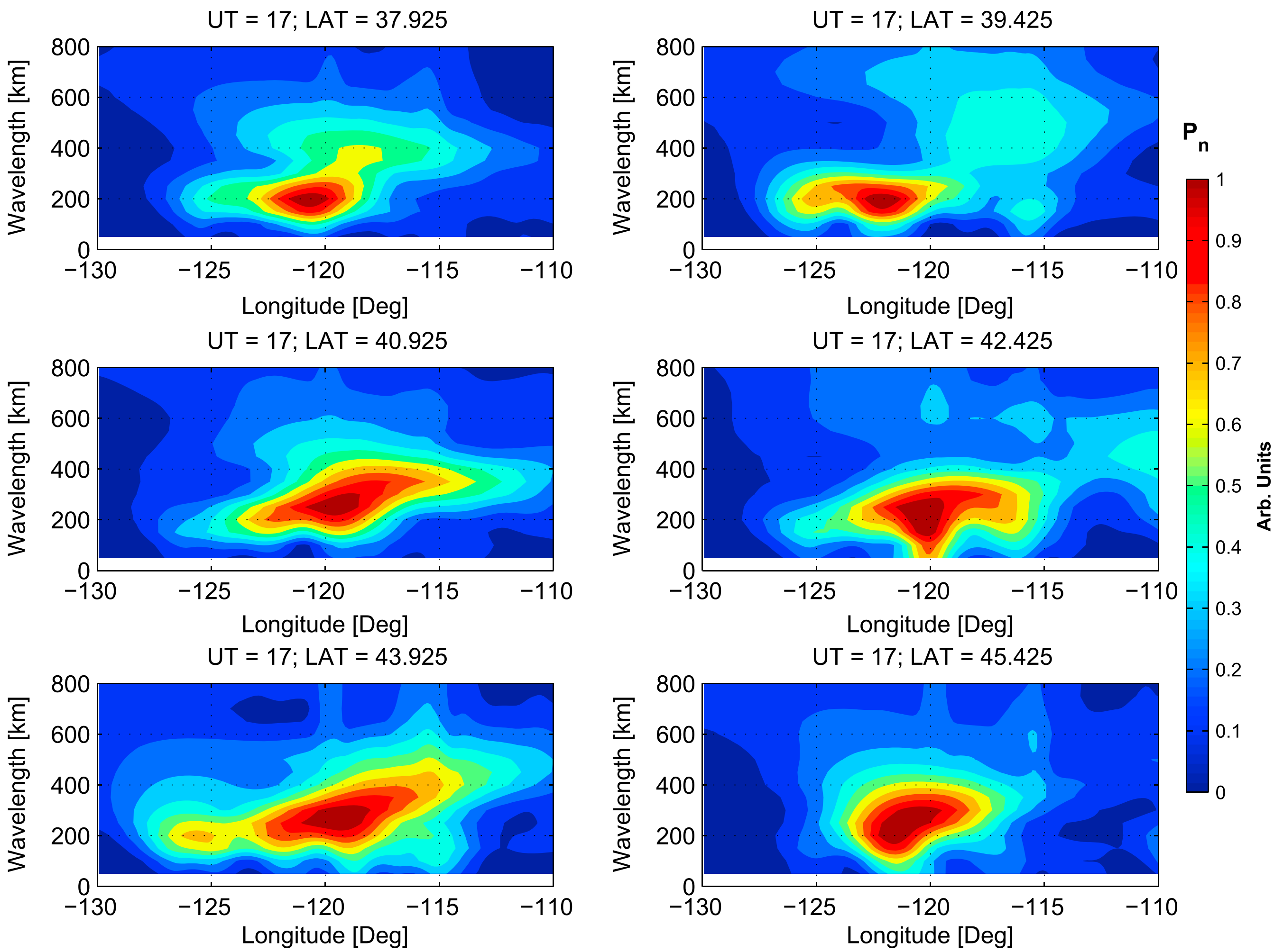

Figure 6. Normalized wavelet spectrogram of the TID horizontal wavelength as a function of longitude for the same latitudes as shown in Figure 5.

AGWs dissipating at $z_{\mathrm{diss}} \sim 225$ km (for example) with $\lambda_H > 100$ km in Figure 4c from *Vadas* [2007]. (Here z_{diss} denotes the altitude where an AGW's momentum flux is maximum. Above this altitude, the AGW's momentum flux decreases rapidly with altitude due to molecular viscosity and thermal diffusivity.) As the intrinsic wave period increases along this line, λ_H and the initial AGW vertical wavelength (y axis of that figure) also increase. Therefore, in order for an AGW with a larger period to have its momentum flux be maximum at the same altitude (e.g., $z_{\mathrm{diss}} \sim 225$ km) as an AGW with a smaller period, the larger-period wave must have a correspondingly larger λ_H and $|\lambda_z|$. Because the period of the TIDs increases with longitude (see Figure 5), λ_H must therefore also increase in longitude to be consistent with AGW dissipative theory.

In fact, the dependence of the wave period with longitude can yield information about the sources of the AGWs. As mentioned previously,

$$\sin(\xi) \sim t_B/t \tag{1}$$

in the zero-wind limit, where ξ is the angle between the horizontal and the direction of propagation of the AGW and τ_B is the buoyancy period [e.g., *Vadas et al.*, 2009]. Using an average buoyancy period between $z \sim 0$ to 250 km of τ_B ~8 min, we find that $\xi \sim 53°$ for AGWs with $\tau = 10$ min and $\xi \sim 19°$ for AGWs with $\tau = 25$ min. For a given oblique propagation angle of ξ, if the vertical distance traveled by an AGW is Δz, then the horizontal distance traveled simultaneously is given by

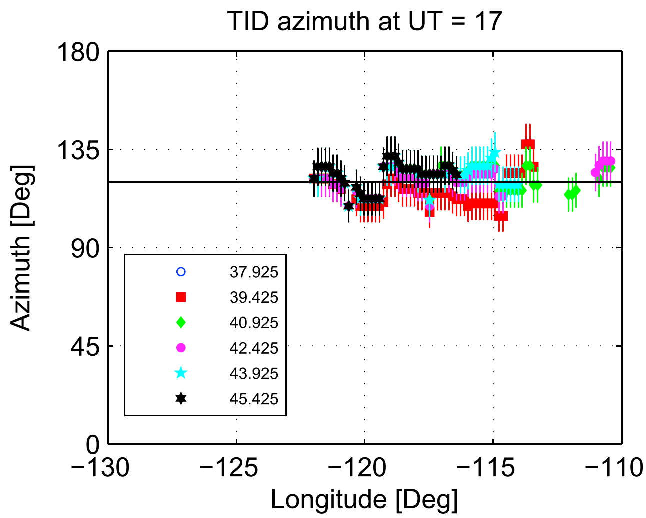

Figure 7. TID azimuths for various latitudes as a function of longitude. Positive values represent angles east of north. The error bars represent 1σ standard deviation in azimuths estimated by propagating the uncertainties in calculated zonal and meridional wave numbers. Different colored symbols represent different latitudes which are identified in the legend box. The solid line drawn at 120° azimuth represents the propagation direction of the tsunami wave near the U.S. Pacific coast as seen in the NOAA tsunami traveltime map shown in Figure 2.

$$x_H \sim \Delta z / \tan(\xi) \tag{2}$$

Assuming the F_2 peak to be at $z = 250$ km (see Figure 1) and using equation (2), we obtain $x_H \sim 190$ km for the AGWs with $\tau = 10$ min and $x_H \sim 730$ km for the AGWs with $\tau = 25$ min. Since the distance between 1° in longitude at 40°N is ~85 km, the horizontal distances traveled by the 10 min and 25 min AGWs are ~2.2° and 9° in longitude, respectively. This rough estimate puts the sources for both GWs just west of the western coast of the U.S. This strongly supports our hypothesis that the tsunami generated the observed TIDs/AGWs as it approached the western coastline of the United States.

The TEC perturbation maps also allow us to calculate the propagation direction of the TIDs. Figure 7 shows the measured TID azimuths (eastward from north) at six different geographic latitudes (different colors) at 17 UT as a function of longitude. The results indicate that on average the TIDs propagated consistently at an angle of 121.8° east of north (solid black line), irrespective of longitude. Comparing this with the angle determined from Figure 2, we see that the azimuths of the TIDs agree very well with the predicted azimuth angle of ~120° of the tsunami near the U.S. Pacific Northwest coast as obtained from NOAA model. This also strongly supports our hypothesis that the tsunami generated the observed TIDs/AGWs.

Next, we compute the horizontal phase speeds of the TIDs, c_H, by tracking the AGW phase fronts in GPS TEC maps and estimating the distance traveled in 20 min. The phase speeds of the TIDs are shown in Figure 8 as a function of longitude for various latitudes. We see that c_H increases slightly with longitude; the phase speeds are ~180–220 m/s at the western edge of the U.S. and ~200–260 m/s at 118°W. Because the smallest sound speed, c_s, in the lower atmosphere is ~260–280 m/s (near the mesopause), we postulate that all of the AGWs shown in Figure 8 could have propagated from the ocean surface (neglecting wind effects). This general statement arises from the fact that the group velocity of an AGW cannot be larger than the sound speed. But, in fact, the AGW dispersion relation is slightly more restrictive. From equation (11) of *Vadas and Crowley* [2010], the maximum intrinsic phase speed (c_{IH}) allowable for an AGW is given by

$$c_{IH}(\max) = 2HN_B \tag{3}$$

where H is the neutral density scale height and N_B is the buoyancy frequency. This expression arises from the anelastic AGW dispersion relation [e.g., *Vadas and Crowley*, 2010, equation (5)]. We assume an approximately isothermal atmosphere, so that $c_s^2 = \gamma g H$ and $N_B^2 = (\gamma - 1)g^2/c_s^2$ [*Vadas*, 2013, equations (21) and (27)]. Then equation (3) becomes

$$c_{IH}(\max) = \left(2\sqrt{\gamma - 1}/\gamma\right)c_s \tag{4}$$

Since $\gamma = 1.4$ in the lower atmosphere [*Kundu*, 1990], we obtain c_{IH} (max) = (0.9)c_s. For $c_s \approx 280$ m/s, the maximum allowable intrinsic phase speed for an AGW in the lower atmosphere is c_{IH} (max) = 255 m/s. This value is in good agreement with the largest calculated phase speed seen in Figure 8, neglecting wind effects near the mesopause (so that the observed phase speed approximately equals the intrinsic phase speed). The slight increase of the horizontal phase speed with longitude (seen in Figure 8) is also consistent with the AGW dissipative theory. If we compare and contrast the $z_{\mathrm{diss}} \sim 225$ km curves in Figures 4c and 5c from *Vadas* [2007],

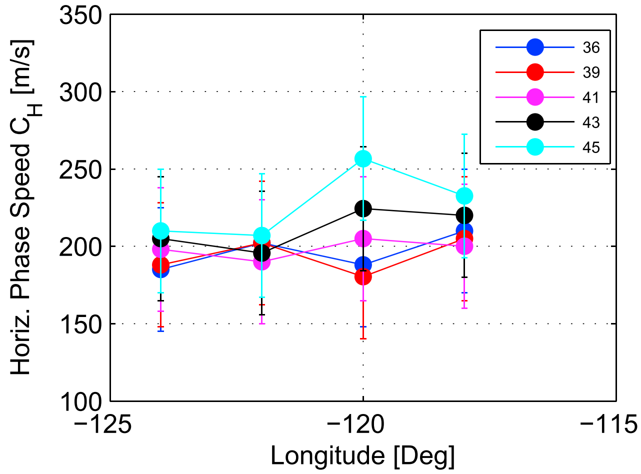

Figure 8. Calculated TID horizontal phase speeds for various latitudes shown here as a function of longitude. The error bars represent 1σ standard deviation computed by propagating the uncertainties in wave periods and horizontal wave numbers. Latitudes are identified in the legend.

we see that c_H increases along this curve (i.e., as λ_H and τ increase). Therefore, the result that the horizontal phase speed increases somewhat with longitude in Figure 8 is consistent with dissipative AGW theory and the tsunami being the source of the observed TIDs/AGWs.

5. Reverse Ray Trace

Observations of TIDs raise an important question of their genesis. The presence of TIDs in the atmosphere after the Tohoku earthquake calls into question whether the source was the earthquake or the tsunami that traveled across the ocean. Near the epicenter, the observed ionospheric perturbations are a mix of waves generated by the earthquake and tsunami [*Galvan et al.*, 2012]. The observations of TIDs presented in this paper are somewhat unique because they were made far away from the epicenter and when the underlying tsunami was abruptly stopped by the land thereby removing the AGW source. We use the 3-D reverse ray trace model described in section 3 to determine the source of the TIDs. We utilize background neutral winds and temperature from a combined ECMWF/TIMEGCM model on 3 March 2011 at 16:30 UT over the region 27.5°N–57.5°N and 100°W–130°W. For $z < 25$ km, we utilize the ECMWF ERA-Interim GRIB data (available at http://rda.ucar.edu). For $35 < z < 600$ km, we utilize TIMEGCM model results [*Roble and Ridley*, 1994] with 5° horizontal resolution. We linearly interpolate the values for $25 < z < 35$ km.

We reverse ray trace 241 observed AGWs backward in time from $z = 250$ km at the same six latitudes shown in Figures 5 and 6 and over a longitude domain between 110°W and 130°W. We stop each calculation when the AGW reflects vertically. The starting and terminal points of the raypaths are shown in Figure 9, and the raypaths for each AGW are shown in Figure 10. We also reverse ray-traced AGWs for zero wind in order to assess the magnitude of the errors associated with the wind (which is the largest component of the error) and find that the results are nearly the same as in Figures 9 and 10 (not shown). In almost every case, the source appears to be located somewhat west of the Pacific coast of the U.S. This is a very strong indication that the source of the AGWs is likely the tsunami as it approached the U.S. coastline.

6. Discussions

During a tsunami, the horizontally travelling surface ocean wave forces the atmosphere [*Daniels*, 1952]. This forcing at the ocean-atmosphere interface excites internal AGWs that can propagate vertically to higher altitudes. Additionally, *Peltier and Hines* [1976] theorized that these tsunami-driven AGWs can create variations in the ionospheric electron density. Similar perturbations of the ionosphere are generated by the seismic source itself, resulting in a rich spectrum of AGWs close to the epicenter. However, farther from the source, only tsunami-driven AGWs can be observed in the ionosphere. Although it is not well known how far or how long these waves persist in the upper atmosphere after the source (i.e., the tsunami) is “removed,” a recent modeling study by *Vadas et al*. [2015] of AGWs excited by an ocean surface wave packet shows that the response at $z = 250$ km at a specific location lasts for 2–4 h. Additionally, that study showed that the fastest AGWs arrive 70–80 min after excitation at the ocean surface. The 2011 tsunami event, and especially the observation of TIDs over the West Coast of the U.S., provided a unique natural experiment to study this aspect of tsunami-ionosphere coupling.

In this section we demonstrate that the TID measurements presented in this paper and the derived results (shown in Figures 4–8) are consistent with dissipative AGW theory. As mentioned previously, Figures 5 and 6

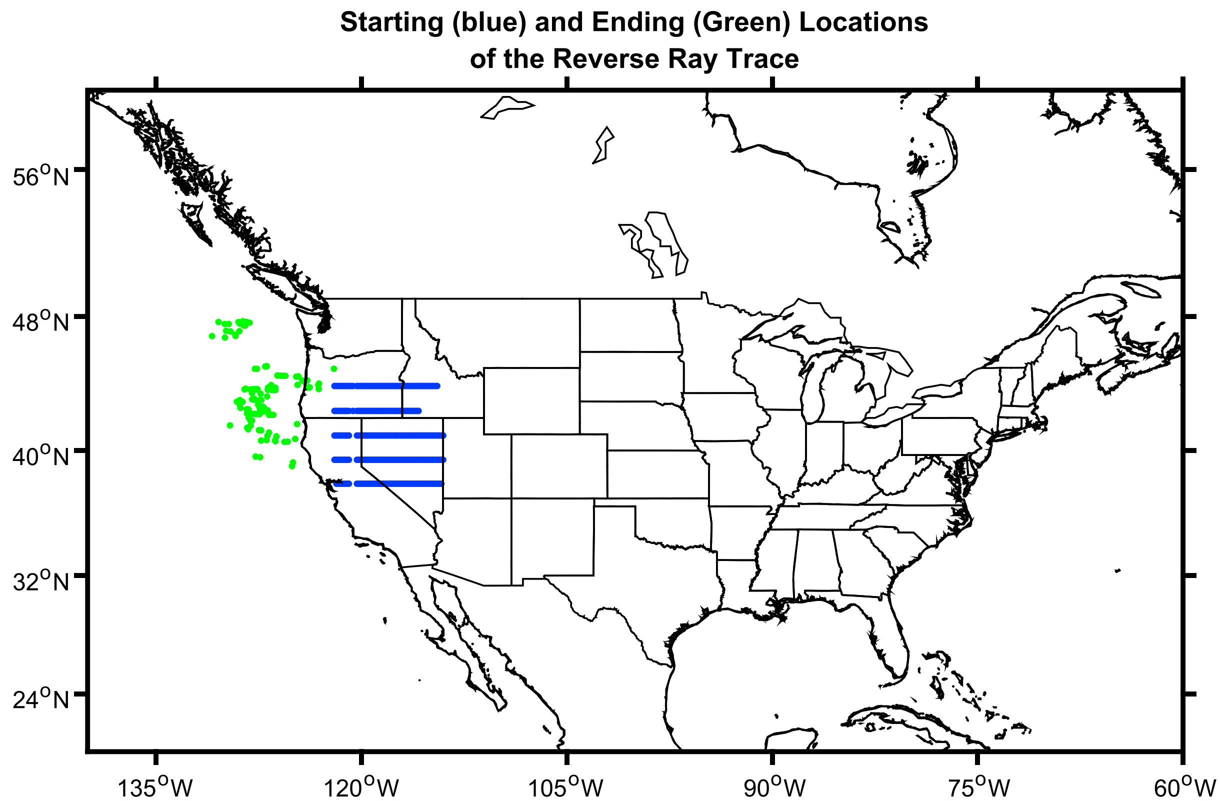

Figure 9. Reverse ray trace results using the combined ECMWF and TIMEGCM winds and temperatures on 11 March 2011 at 16:30 UT. The blue symbols represent the locations of the starting points of the reverse ray tracing at $z = 250$ km. The green symbols represent the locations of the raypaths at their minimum altitude during the reverse ray tracing.

show that the maximum TEC perturbations occur for waves with $\tau = 12$–16 min and λ_H ~150–250 km. The IRI model results (Figure 1) show that the bottomside of the *F* layer is at $z \sim 150$–200 km. Additionally, the model profiles also indicate that the *F* layer peaks at $z \sim 250$–260 km and has a thickness of $z \sim 150$–250 km. For an ionosphere with these *F* layer characteristics we expect that in order for the neutrals to drag the ions and create significant electron density perturbations, the AGWs must have momentum fluxes that peak at altitudes of $z_{\rm diss} \sim 200$–250 km or higher (based on the previous work by *Vadas* [2007]). Figure 4c from *Vadas* [2007] shows $z_{\rm diss}$ for a temperature profile representative of the conditions on 11 March 2011 over western U.S. (i.e., having an exospheric temperature of 1000 K). For an AGW with $\tau = 12$–16 min and λ_H ~150–250 km, we see from Figure 4c of *Vadas* [2007] that $z_{\rm diss} \sim 200$–250 km. Additionally, the amplitude of an AGW can be significant up to $z = z_{\rm diss} + H$ [*Vadas*, 2007]. Using the NRLMSIS-000 model [*Picone et al.*, 2002], we estimate the neutral density scale height (H) to be ~32–42 km for this height range. Therefore, we assert that AGWs with periods of 12–16 min and λ_H ~150–250 km can propagate to $z \sim z_{\rm diss} + H \sim 230$–290 km and still be observed. Thus, we conclude that the AGWs generated by the tsunami propagated to at least the bottomside of the *F* layer and likely propagated to the peak of the *F* layer.

To verify the causal relationship between the tsunami and the observed TIDs, we investigate the perturbation envelope of the ocean surface as measured by a buoy deployed in the Pacific. Figure 11 shows the 15 s Bottom Pressure Recorded (BPR) data from a Deep-ocean Assessment and Reporting of Tsunami (DART) buoy in the East Pacific region (located at 39.328°N and 127.013°W, just west of the northern coast of California) on 11 March 2011 and the corresponding spectrogram. At 15 UT the onset of the tsunami wave is clearly discernible in the raw BPR data. The spectrogram of the BPR data suggests that the tsunami at the location of the buoy generated ocean surface perturbations with periods ranging from 10 to 70 min, with most of the signal occurring at $\tau = 10$–30 min and $\tau = 40$–55 min. These shorter periods overlap with the wave periods in the TEC data (10 to 30 min from Figure 5), although the peak periods differ. Specifically, the peak from the DART buoy (Figure 11b) is at $\tau = 27$ min, with a smaller but significant peak at $\tau = 22$ min, whereas the peak in the TEC data

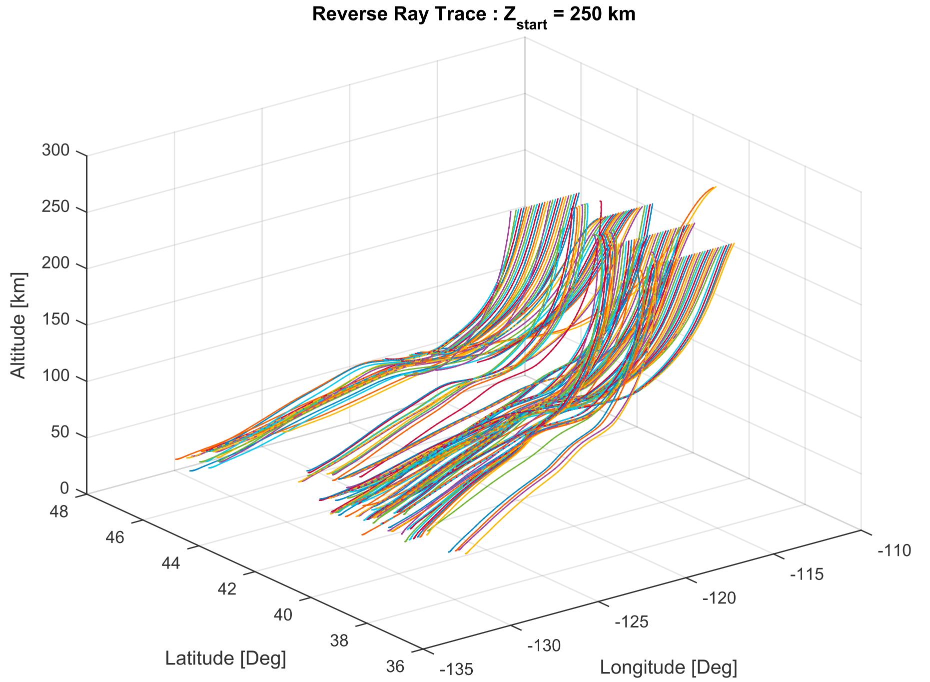

Figure 10. Raypaths of the AGW considered in the reverse ray tracing. The rays were traced back in time starting at the F_2 peak height, which from Figure 1 was at 250 km.

is at $\tau = 12–16$ min, with a smaller peak at $\tau = 20$ min for 37.9° and 39.4°N (see Figure 5). The shift of the peak of the AGW spectrum from larger to smaller periods in the thermosphere occurs because of the dissipative filtering of AGWs from molecular viscosity, as has been observed in recent modeling studies for the propagation and dissipation of AGWs excited by ocean surface wave packets [*Vadas et al*., 2015]. We discuss this shift in detail below. Additionally, we caution the reader that although the spectrogram generated from the BPR data shown in Figure 11 does peak at longer periods, it is not known what length scales these periods correspond to. If the length scales are smaller than 100 km, then the excited AGWs could not propagate very far into the thermosphere before dissipating [*Vadas*, 2007].

Figure 11 shows that the largest-amplitude wave observed in the DART buoy data had a period of 27 min, whereas the peak period of the TIDs in TEC data was 12–16 min from Figure 5. If the ocean waves had horizontal wavelengths of several hundred kilometers, then this would imply that the peak of the AGW spectrum shifted from ~27 min to ~12–16 min from the troposphere to the *F* layer. Such a behavior can be easily explained by dissipative AGW theory. Indeed, a similar spectral shift occurred for AGWs excited by an ocean surface wave packet in a recent modeling study; in that study, the peak period shifted from $\tau \sim 20$ min at the ocean surface to $\tau \sim 15$ min the thermosphere at $z = 250$ km [*Vadas et al*., 2015]. This occurred because the shorter-period AGWs had larger vertical wavelengths and were, therefore, able to propagate deeper into the thermosphere prior to dissipation. For example, from Figure 4c of *Vadas* [2007], the altitude where the momentum flux attains its maximum value for AGWs with $\tau = 27$ min and λ_H ~150–250 km is between 150 and 185 km. The density scale height (H) in this altitude region is ~15–25 km. If these long-period waves in the DART data had λ_H ~150–250 km, then we would conclude that these AGWs could have barely reached the bottomside of the *F* layer before dissipating from molecular viscosity. This explains why the 27 min waves seen in the DART data could not have significantly perturbed the electron density and were, therefore, not seen in the TEC data. In fact, as shown in *Vadas et al*. [2015], the thermosphere significantly enhances the relative amplitudes of the shorter-period ($\tau = 13–15$ min) AGWs because they have larger λ_z and can therefore penetrate deeper into the thermosphere prior to being damped by molecular viscosity. Indeed, *Vadas et al*. [2015] found that the shorter-period AGWs had $\lambda_z \sim 250$ km, while the longer-period AGWs had $\lambda_z \sim 80$ km. Not only are the longer-period AGWs suppressed at $z = 250$ km because of viscous dissipation, but they are also suppressed because they are

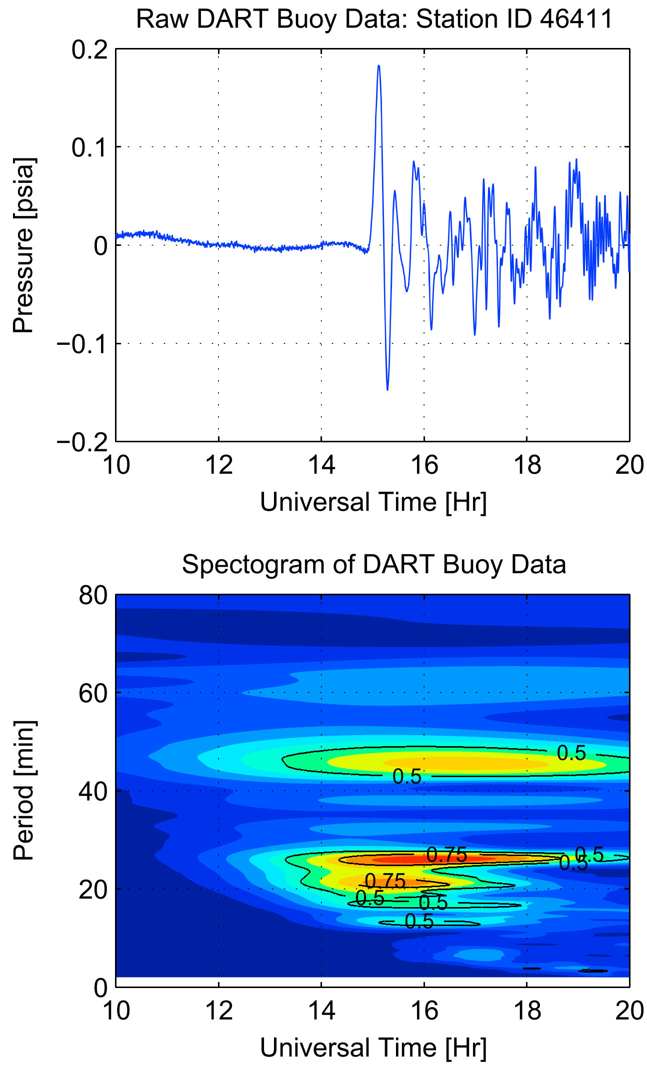

Figure 11. (top) The 15 s Bottom Pressure Recorded data from a DART buoy located at 39.328°N and 127.013°W in the East Pacific region on 11 March 2011 and (bottom) the corresponding normalized wavelet power spectrogram showing the spectral content of the tsunami wave approaching the U. S. coastline.

partially or fully averaged out vertically in the integration of the vertical TEC. Therefore, the observation of AGWs here with $\tau = 10$–20 min having large TEC amplitudes is consistent with dissipative AGW theory, because these AGWs can reach the *F* region prior to dissipating with large-enough vertical wavelengths so as to be observed in the TEC.

Next, we discuss the sharp cutoff of the observed TIDs east of 112°W longitude. Recall Figure 11 which shows the spectrum of the DART buoy data with significant power at larger periods near ~40–55 min. The wavelet spectrum in Figure 11 suggests that AGWs with periods of 40–55 min could have been excited by the tsunami as it approached the West Cost of the U.S. (although again, λ_H is unknown). From equations (3) and (4), for an AGW with a period of 55 min, the horizontal distance traveled during the time it takes to propagate 250 km vertically (from the ocean surface) is approximately ~180–200 km. This corresponds to eastern Wyoming/Colorado/New Mexico. However, no signatures of AGWs are seen in the TEC data over this region (see Figure 4). Instead, there is a sharp cutoff in TIDs at ~112°W (see Figure 4). Using equations (1) and (2), we estimate that the maximum period an AGW can have that propagates horizontally to 112°W is $\tau \sim 36$ min. From Figure 4c of *Vadas* [2007], an AGW with $\tau \sim 36$ min and λ_H ~150–400 km has $z_{\text{diss}} \sim 130$–190 km. Such an AGW could have a significant amplitude only up to $z \sim z_{\text{diss}} + H$ (~140–230 km), which is in the bottomside of the *F* layer where the electron density is small. Therefore, AGWs with $\tau \sim 36$ min are likely the largest-period AGWs that can significantly perturb the *F* layer and generate TEC perturbations. Any AGWs with larger τ excited by the tsunami would still propagate over South Dakota/Nebraska/Oklahoma but would not likely reach the *F* region and significantly perturb the ionosphere.

Finally, we consider the possibility that the observed AGWs might have been created by a different source. There are very few known sources which excite medium-scale AGWs having linear phase lines oriented in approximately the north-south direction and having horizontal phase speeds of ~200 m/s. One such source might be mountain waves (in this case from the Sierra Nevada Mountains on the West Coast of the U.S.). However, mountain waves have near-zero phase speeds. Another source might be the secondary AGWs excited by the body forces created by the dissipation of mountain waves [*Smith et al.*, 2013]. However, if this were the source, then it is difficult to understand why these AGWs are not seen regularly in the TEC in the western portion of the U.S. Additionally, the AGW phase lines would be approximately parallel to the mountain chain in this case (i.e., tilted west of north). This tilt is opposite to the tilt of the phase lines for the TIDs observed here, which is east of north. Finally, the solar terminator also creates AGWs with an angle of 30° to the terminator [*Forbes et al*., 2008; *Liu et al*., 2009]. However, these waves have horizontal wavelengths of ~1000 km or more and are created around sunset and sunrise. These horizontal scales are far larger than those observed here. Therefore, we conclude that the tsunami is the only reasonable source which could explain the properties of the observed TIDs/AGWs.

7. Conclusions

In this paper, using the dense network of GPS measurements over the U.S., we demonstrate that the 2011 tsunami-generated TIDs persisted for about 4 h over North America. During that time, the TIDs propagated more than 1000 km inland. Spectral analysis of the TIDs indicates that the period and horizontal wavelength of the TEC disturbances increased with distance from the West Coast of the U.S. to Colorado/Wyoming, which agrees with dissipative AGW theory and their source being the tsunami. This suggests that tsunami-generated AGWs can persist for several hours and travel a thousand kilometers after their source has "been removed."

The observational results presented here are consistent with a recent study which modeled a short-duration (localized-in-time) ocean surface wave packet that ended at a given time and therefore excited no additional AGWs [*Vadas et al*., 2015]; this is similar to the present scenario where the Tohoko tsunami stopped at the West Coast of the U.S. and therefore stopped exciting AGWs at that location and time. *Vadas et al*. [2015] found that the AGWs excited by the ocean surface wave packet propagated up to $z = 250$ km at distances ~250 to ~1000–1200 km horizontally from their excitation location and that the response in the thermosphere lasted for 2.5–4 h (Figures 11 and 17 of that work). The horizontal range was found to be limited to ~1000–1200 km because the larger-period AGWs (which travel farther horizontally) dissipated from viscosity below $z = 250$ km. It was also found that only those AGWs with $\tau < 35$ min were visible at $z = 250$ km (Figures 10 and 16 of that work).

The connection between tsunamis and ionospheric perturbations was speculated in the 1970s by *Peltier and Hines* [1976]. They demonstrated theoretically that tsunamis can excite AGWs, which are capable of propagating vertically into the ionosphere and creating variations in the electron density. It is now known that the structure of the ionosphere can be perturbed during seismic events and associated tsunamis; however, the full extent of the multiscale dynamical processes operating between the neutral atmosphere and ionosphere is not understood. There is a growing interest in ionospheric detection of seismic events and tsunamis [*Occhipinti et al*., 2008b; *Artru et al*., 2005]. However, the realization of a tsunami warning system that is based on ionospheric monitoring requires more work to advance our understanding of the coupling processes between the atmosphere and ionosphere. Additional measurements of tsunami-related ionospheric signatures will serve to provide new scientific insights into the geophysical source phenomenology. The measurements will also enable fundamental investigations of wave propagation and dissipation, leading in turn to deeper insights into the conditions under which ocean-atmosphere coupling is effective. The GPS TEC observations presented here demonstrate the transport of wave energy and momentum over large distances and the morphological characteristics of the TIDs/AGWs. This study shows that the network of ground-based GPS receivers can be extremely useful in providing deeper insights concerning the full chain of coupled plasma processes in the atmosphere-ionosphere system.

Acknowledgments
Data and model output are available from the corresponding author on request. This work was supported by the ONR award FA9550-07-1-0565, NASA contract NNH13CJ33C, and National Science Foundation grant AGS-1552310 to ASTRA and ONR grant N00014-13-1-0350 to the University of Illinois. S.L.V. was supported by ONR grant N00014-13-1-0475, NASA contract NNH12CE58C, and NSF grant AGS-1552315. We acknowledge the use of publicly available ground-based GPS TEC data from the Southern California Integrated GPS Network, International GPS Service for Geodynamics, UNAVCO, Hartebeesthoek Radio Astronomy Observatory, Natural Resources Canada, Geoscience Australia, the Brazilian Institute of Geography and Statistics, University of New Brunswick, National Oceanic and Atmospheric Administration, and National Aeronautics and Space Administration.

References

Alexander, M. J. (1996), A simulated spectrum of convectively generated gravity waves: Propagation from the tropopause to the mesopause and effects on the middle atmosphere, *J. Geophys. Res.*, *101*, 1571–1588, doi:10.1029/95JD02046.

Alexander, M. J., J. R. Holton, and D. R. Durran (1995), The gravity wave response above deep tropical convection in a squall line simulation, *J. Atmos. Sci.*, *52*(12), 2212–2226, doi:10.1175/1520-0469(1995)052<2212:TGWRAD>2.0.CO;2.

Artru, J., V. Ducic, H. Kanamori, P. Lognonń e, and M. Murakami (2005), Ionospheric detection of gravity waves induced by tsunamis, *Geophys. J. Int.*, *160*, 840–848, doi:10.1111/j.1365-246X.2005.02552.x.

Astafyeva, E., P. Lognonné, and L. Rolland (2011), First ionospheric images of the seismic fault slip on the example of the Tohoku-oki earthquake, *Geophys. Res. Lett.*, *38*, L22104, doi:10.1029/2011GL049623.

Azeem, I., J. Yue, L. Hoffmann, S. D. Miller, W. C. Straka III, and G. Crowley (2015), Multisensor profiling of a concentric gravity wave event propagating from the troposphere to the ionosphere, *Geophys. Res. Lett.*, *42*, doi:10.1002/2015GL065903.

Bilitza, D., D. Altadill, Y. Zhang, C. Mertens, V. Truhlik, P. Richards, L.-A. McKinnell, and B. Reinisch (2014), The International Reference Ionosphere 2012—A model of international collaboration, *J. Space Weather Space Clim.*, *4*, 1–12, doi:10.1051/swsc/2014004.

Bowman, G. G. (1990), A review of some recent work on mid-latitude spread-*F* occurrence as detected by ionosondes, *J. Geomag. Geoelectr.*, *42*, 109–138, doi:10.5636/jgg.42.109.

Broutman, D., S. D. Eckermann, and D. P. Drob (2014), The partial reflection of tsunami-generated gravity waves, *J. Atmos. Sci.*, *71*, 3416–3426, doi:10.1175/JAS-D-13-0309.1.

Crowley, G., and F. S. Rodrigues (2012), Characteristics of traveling ionospheric disturbances observed by the TIDDBIT sounder, *Radio Sci.*, *47*, RS0L22, doi:10.1029/2011RS004959.

Crowley, G., and I. W. McCrea (1988), A synoptic study of TIDs observed in the UK during the first WAGS campaign, October 10–18, 1985, *Radio Sci.*, *23*, 905–917, doi:10.1029/RS023i006p00905.

Crowley, G., T. B. Jones, and J. R. Dudeney (1987), Comparison of short period TID morphologies in Antarctica during geomagnetically quiet and active intervals, *J. Atmos. Terr. Phys.*, *49*, 1155–1162, doi:10.1016/0021-9169(87)90098-5.

Crowley, G., I. Azeem, A. Reynolds, T. M. Duly, P. McBride, C. Winkler, and D. Hunton (2016), Analysis of traveling ionospheric disturbances (TIDs) in GPS TEC launched by the 2011 Tohoku earthquake, *Radio Sci.*, *51*, 507–514, doi:10.1002/2015RS005907.

Daniels, F. B. (1952), Acoustical energy generated by the ocean waves, *J. Acoust. Soc. Am.*, *24*(1), 83.

Del Genio, A. D., G. Schubert, and J. M. Straus (1979), Gravity wave propagation in a diffusively separated atmosphere with height-dependent collision frequencies, *J. Geophys. Res.*, *84*(A8), 4371–4378, doi:10.1029/JA084iA08p04371.

Dewan, E. M., R. H. Picard, R. R. ONeil, H. A. Gardiner, J. Gibson, J. D. Mill, E. Richards, M. Kendra, and W. O. Gallery (1998), MSX satellite observations of thunderstorm-generated gravity waves in mid-wave infrared images of the upper stratosphere, *Geophys. Res. Lett.*, *25*, 939–942, doi:10.1029/98GL00640.

Duly, T. M., N. P. Chapagain, and J. J. Makela (2013), Climatology of nighttime medium-scale traveling ionospheric disturbances (MSTIDs) in the Central Pacific and South American sectors, *Ann. Geophys.*, *31*, 2229–2237, doi:10.5194/angeo-31-2229-2013.

Duly, T. M., J. D. Huba, and J. J. Makela (2014), Self-consistent generation of MSTIDs within the SAMI3 numerical model, *J. Geophys. Res. Space Physics*, *119*, 6745–6757, doi:10.1002/2014JA020146.

Forbes, J. M., S. L. Bruinsma, Y. Miyoshi, and H. Fujiwara (2008), A solar terminator wave in thermosphere neutral densities measured by the CHAMP satellite, *Geophys. Res. Lett.*, *35*, L14802, doi:10.1029/2008GL034075.

Fovell, R., D. Durran, and J. R. Holton (1992), Numerical simulations of convectively generated stratospheric gravity waves, *J. Atmos. Sci.*, *49*, 1427–1442, doi:10.1175/1520-0469(1992)049<1427:NSOCGS>2.0.CO;2.

Francis, S. H. (1975), Global propagation of atmospheric gravity waves: A review, *J. Atmos. Sol. Terr. Phys.*, *37*, 1031–1054.

Fraser, S., G. S. Leonard, I. Matsuo, and H. Murakami (2012), Tsunami evacuation: Lessons from the Great East Japan earthquake and tsunami of March 11th 2011, GNS Sci. Rep. 2012/17, 89 p.

Fujii, Y., K. Satake, S. Sakai, M. Shinohara, and T. Kanazawa (2011), Tsunami source of the 2011 off the Pacific coast of Tohoku Earthquake, *Earth Planets Space*, *63*, 815–820, doi:10.5047/eps.2011.06.010.

Fukushima, D., K. Shiokawa, Y. Otsuka, and T. Ogawa (2012), Observation of equatorial nighttime medium-scale traveling ionospheric disturbances in 630-nm airglow images over 7 years, *J. Geophys. Res.*, *117*, A10324, doi:10.1029/2012JA017758.

Galvan, D. A., A. Komjathy, M. P. Hickey, and A. J. Mannucci (2011), The 2009 Samoa and 2010 Chile tsunamis as observed in the ionosphere using GPS total electron content, *J. Geophys. Res.*, *116*, A06318, doi:10.1029/2010JA016204.

Galvan, D. A., A. Komjathy, M. P. Hickey, P. Stephens, J. Snively, Y. Tony Song, M. D. Butala, and A. J. Mannucci (2012), Ionospheric signatures of Tohoku-Oki tsunami of March 11, 2011: Model comparisons near the epicenter, *Radio Sci.*, *47*, RS4003, doi:10.1029/2012RS005023.

Garcia, F. J., M. C. Kelley, J. J. Makela, and C.-S. Huang (2000), Airglow observations of mesoscale low-velocity traveling ionospheric disturbances at midlatitudes, *J. Geophys. Res.*, *105*, 18,407–18,415, doi:10.1029/1999JA000305.

Garcia, R. F., E. Doornbos, S. Bruinsma, and H. Hebert (2014), Atmospheric gravity waves due to the Tohoku-Oki tsunami observed in the thermosphere by GOCE, *J. Geophys. Res. Atmos.*, *119*, 4498–4506, doi:10.1002/2013JD021120.

Gossard, E. E., and W. H. Hooke (1975), *Waves in the Atmosphere*, pp. 456, Elsevier Scientific Publ. Co., Amsterdam.

Hasbi, A. M., M. A. Mohd Ali, and N. Misran (2011), Ionospheric variations before some large earthquakes over Sumatra, *Nat. Hazards Earth Syst. Sci.*, *11*, 597–611, doi:10.5194/nhess-11-597-2011.

Heale, C. J., J. B. Snively, M. P. Hickey, and C. J. Ali (2014), Thermospheric dissipation of upward propagating gravity wave packets, *J. Geophys. Res. Space Physics*, *119*, 3857–3872, doi:10.1002/2013JA019387.

Hickey, M. P., and K. D. Cole (1988), A numerical model for gravity wave dissipation in the thermosphere, *J. Atmos. Terr. Phys.*, *50*, 689–697, doi:10.1016/0021-9169(88)90032-3.

Hickey, M. P., G. Schubert, and R. L. Walterscheid (2010), Atmospheric airglow fluctuations due to a tsunami-driven gravity wave disturbance, *J. Geophys. Res.*, *115*, A06308, doi:10.1029/2009JA014977.

Hines, C. O. (1960), Internal atmospheric gravity waves at ionospheric heights, *Can. J. Phys.*, *38*, 1441–1481, doi:10.1139/p60-150.

Hines, C. O. (1967), On the nature of travelling ionospheric disturbances launched by low-altitude nuclear explosions, *J. Geophys. Res.*, *72*, 1877–1882, doi:10.1029/JZ072i007p01877.

Hocke, K., and K. Schlegel (1996), A review of atmospheric gravity waves and travelling ionospheric disturbances: 1982–1995, *Ann. Geophys.*, *14*, 917–940.

Holton, J. R., and M. J. Alexander (1999), Gravity waves in the mesosphere generated by tropospheric convection, *Tellus A-B*, *51*, 45–58, doi:10.3402/tellusb.v51i1.16259.

Hooke, W. H. (1968), Ionospheric irregularities produced by internal atmospheric gravity waves, *J. Atmos. Terr. Phys.*, *30*, 795–823, doi:10.1016/S0021-9169(68)80033-9.

Hunsucker, R. D. (1982), Atmospheric gravity waves generated in the high-latitude ionosphere: A review, *Rev. Geophys.*, *20*, 293–315, doi:10.1029/RG020i002p00293.

Kaplan, E. D., and C. Hagerty (2006), *Understanding GPS: Principles and Applications*, 2nd ed., Artech House, Inc., Norwood, Mass.

Kelley, M. C., and C. A. Miller (1997), Electrodynamics of midlatitude spread *F*: 3. Electrohydrodynamic waves? A new look at the role of electric fields in thermospheric wave dynamics, *J. Geophys. Res.*, *102*, 11,539–11,547, doi:10.1029/96JA03841.

Kelley, M. C., and S. Fukao (1991), Turbulent upwelling of the mid-latitude ionosphere: 2. Theoretical framework, *J. Geophys. Res.*, *96*, 3747–3753, doi:10.1029/90JA02252.

Kelley, M. C., J. J. Makela, W. E. Swartz, S. C. Collins, S. Thonnard, N. Aponte, and C. A. Tepley (2000), Caribbean Ionosphere Campaign, year one: Airglow and plasma observations during two intense mid-latitude spread-*F* events, *Geophys. Res. Lett.*, *27*, 2825–2828, doi:10.1029/2000GL000022.

Kherani, E. A., M. A. Abdu, E. R. de Paula, D. C. Fritts, J. H. A. Sobral, and F. C. de Meneses Jr. (2009), The impact of gravity waves rising from convection in the lower atmosphere on the generation and nonlinear evolution of equatorial bubble, *Ann. Geophys.*, *27*, 1657–1668, doi:10.5194/angeo-27-1657-2009.

Kundu, P. (1990), *Fluid Mechanics*, pp. 638, Academic Press, San Diego, Calif.

Lane, T. P., M. J. Reeder, and T. L. Clark (2001), Numerical modeling of gravity wave generation by deep tropical convection, *J. Atmos. Sci.*, *58*, 1249–1274, doi:10.1175/1520-0469(2001)058<1249:NMOGWG>2.0.CO;2.

Liu, H., H. Luhr, and S. Watanabe (2009), A solar terminator wave in thermospheric wind and density simultaneously observed by CHAMP, *Geophys. Res. Lett.*, *36*, L10109, doi:10.1029/2009GL038165.

Liu, J. Y., Y. B. Tsai, K. F. Ma, Y. I. Chen, H. F. Tsai, C. H. Lin, M. Kamogawa, and C. P. Lee (2006), Ionospheric GPS total electron content (TEC) disturbances triggered by the 26 December 2004 Indian Ocean tsunami, *J. Geophys. Res.*, *111*, A05303, doi:10.1029/2005JA011200.

Liu, J.-Y., C.-H. Chen, C.-H. Lin, H.-F. Tsai, C.-H. Chen, and M. Kamogawa (2011), Ionospheric disturbances triggered by the 11 March 2011 *M*9.0 Tohoku earthquake, *J. Geophys. Res.*, *116*, A06319, doi:10.1029/2011JA016761.

Lognonńe, P., J. Artru, R. Garcia, F. Crespon, V. Ducic, E. Jeansou, G. Occhipinti, J. Helbert, G. Moreaux, and P. Godet (2006), Ground-based GPS imaging of ionospheric postseismic signal, *Planet. Space Sci.*, *54*, 528–540, doi:10.1016/j.pss.2005.10.021.

Makela, J. J., and Y. Otsuka (2011), Overview of nighttime ionospheric instabilities at low- and mid-latitudes: Coupling aspects resulting in structuring at the mesoscale, *Space Sci. Rev.*, *168*(1–4), 419–440.

Makela, J. J., et al. (2011), Imaging and modeling the ionospheric airglow response over Hawaii to the tsunami generated by the Tohoku earthquake of 11 March 2011, *Geophys. Res. Lett.*, *38*, L13305, doi:10.1029/2011GL047860.

Matsumura, M., A. Saito, T. Iyemori, H. Shinagawa, T. Tsugawa, Y. Otsuka, M. Nishioka, and C. H. Chen (2011), Numerical simulations of atmospheric waves excited by the 2011 off the Pacific coast of Tohoku earthquake, *Earth Planets Space*, *63*(7), 885–889, doi:10.5047/eps.2011.07.015.

Meng, X., A. Komjathy, O. P. Verkhoglyadova, Y.-M. Yang, Y. Deng, and A. J. Mannucci (2015), A new physics-based modeling approach for tsunami-ionosphere coupling, *Geophys. Res. Lett.*, *42*, 4736–4744, doi:10.1002/2015GL064610.

Miller, C. A., W. E. Swartz, M. C. Kelley, M. Mendillo, D. Nottingham, J. Scali, and B. Reinisch (1997), Electrodynamics of midlatitude spread *F*: 1. Observations of unstable, gravity wave-induced ionospheric electric fields at tropical latitudes, *J. Geophys. Res.*, *102*, 11,521–11,532, doi:10.1029/96JA03839.

Nicolls, M. J., and C. J. Heinselman (2007), Three dimensional measurements of traveling ionospheric disturbances with the Poker Flat Advanced Modular Incoherent Scatter Radar, *Geophys. Res. Lett.*, *34*, L21104, doi:10.1029/2007GL031506.

Nicolls, M. J., R. H. Varney, S. L. Vadas, P. A. Stamus, C. J. Heinselman, R. B. Cosgrove, and M. C. Kelley (2010), Influence of an inertia-gravity wave on mesospheric dynamics: A case study with the Poker Flat Incoherent Scatter Radar, *J. Geophys. Res.*, *115*, D00N02, doi:10.1029/2010JD014042.

Nicolls, M. J., S. L. Vadas, N. Aponte, and M. P. Sulzer (2014), Horizontal wave parameters of daytime thermospheric gravity waves and *E* region neutral winds over Puerto Rico, *J. Geophys. Res. Space Physics*, *119*, 575–600, doi:10.1002/2013JA018988.

Nishioka, M., T. Tsugawa, M. Kubota, and M. Ishii (2013), Concentric waves and short-period oscillations observed in the ionosphere after the 2013 Moore EF5 tornado, *Geophys. Res. Lett.*, *40*, 5581–5586, doi:10.1002/2013GL057963.

Occhipinti, G., L. Rolland, P. Lognonné, and S. Watada (2013), From Sumatra 2004 to Tohoku-Oki 2011: The systematic GPS detection of the ionospheric signature induced by tsunamigenic earthquakes, *J. Geophys. Res. Space Physics*, *118*, 3626–3636, doi:10.1002/jgra.50322.

Occhipinti, G., P. Lognonné, E. Alam Kherani, and H. Hébert (2006), Three-dimensional waveform modeling of ionospheric signature induced by the 2004 Sumatra tsunami, *Geophys. Res. Lett.*, *33*, L20104, doi:10.1029/2006GL026865.

Occhipinti, G., A. Kherani, and P. Lognonné (2008a), Geomagnetic dependence of ionospheric disturbances induced by tsunamigenic internal gravity waves, *Geophys. J. Int.*, *173*, 753–765, doi:10.1111/j.1365-246X.2008.03760.x.

Occhipinti, G., A. Komjathy, and P. Lognonné (2008b), Tsunami detection by GPS, GPS World, 1 Feb., pp. 50–56.

Occhipinti, G., P. Coisson, J. J. Makela, S. Allgeyer, A. Kherani, H. Hebert, and P. Lognonné (2011), Three-dimensional numerical modeling of tsunami-related internal gravity waves in the Hawaiian atmosphere, *Earth Planets Space*, *63*, 847–851, doi:10.5047/eps.2011.06.051.

Otsuka, Y., K. Shiokawa, and T. Ogawa (2004), Geomagnetic conjugate observations of medium-scale traveling ionospheric disturbances at midlatitude using all-sky airglow imagers, *Geophys. Res. Lett.*, *31*, L15803, doi:10.1029/2004GL020262.

Paulino, I., H. Takahashi, S. L. Vadas, C. M. Wrasse, J. H. A. Sobral, A. F. Medeiros, R. A. Buriti, and D. Gobbi (2012), Forward ray-tracing for medium-scale gravity waves observed during the COPEX campaign, *J. Atmos. Sol. Terr. Phys.*, *90-91*, 117–123, doi:10.1016/j.jastp.2012.08.006.

Paulino, I., et al. (2016), Periodic waves in the lower thermosphere observed by OI630-nm airglow images, *Ann. Geophys.*, *34*, 293–301, doi:10.5194/angeo-34-293-2016.

Peltier, W. R., and C. O. Hines (1976), On the possible detection of tsunamis by a monitoring of the ionosphere, *J. Geophys. Res.*, *81*, 1995–2000.

Picone, J. M., A. E. Hedin, D. P. Drob, and A. C. Aikin (2002), NRLMSISE-00 empirical model of the atmosphere: Statistical comparisons and scientific issues, *J. Geophys. Res.*, *107*(A12), 1468, doi:10.1029/2002JA009430.

Rice, D. D., R. D. Hunsucker, L. J. Lanzerotti, G. Crowley, P. J. S. Williams, J. D. Craven, and L. Frank (1988), Observations of the source and propagation of atmospheric gravity waves, *Nature*, *328*, 231–233.

Richmond, A. D. (1978), Gravity wave generation, propagation, and dissipation in the thermosphere, *J. Geophys. Res.*, *83*, 4131–4145, doi:10.1029/JA083iA09p04131.

Roble, R. G., and E. C. Ridley (1994), A thermosphere-ionosphere-mesosphere electrodynamics general circulation model (TIME-GCM): Equinox solar cycle minimum simulations (30–500 km), *Geophys. Res. Lett.*, *21*, 417–420, doi:10.1029/93GL03391.

Rolland, L. M., G. Occhipinti, P. Lognonné, and A. Loevenbruck (2010), Ionospheric gravity waves detected offshore Hawaii after tsunamis, *Geophys. Res. Lett.*, *37*, L17101, doi:10.1029/2010GL044479.

Rolland, L., P. Lognonne, E. Astafyeva, A. Kherani, N. Kobayashi, M. Mann, and H. Munekane (2011), The resonant response of the ionosphere imaged after the 2011 Tohoku-Oki earthquake, *Earth Planets Space*, *63*, 853–857, doi:10.5047/eps.2011.06.020.

Row, R. V. (1967), Acoustic-gravity waves in the upper atmosphere due to a nuclear detonation and an earthquake, *J. Geophys. Res.*, *72*, 1599–1610, doi:10.1029/JZ072i005p01599.

Saito, A., T. Tsugawa, Y. Otsuka, M. Nishioka, T. Iyemori, M. Matsumura, S. Saito, C. H. Chen, Y. Goi, and N. Choosakul (2011), Acoustic resonance and plasma depletion detected by GPS total electron content observation after the 2011 off the Pacific coast of Tohoku Earthquake, *Earth Planets Space*, *63*, 863–867, doi:10.5047/eps.2011.06.034.

Sentman, D. D., E. M. Wescott, R. H. Picard, J. R. Winick, H. C. Stenbaek-Nielsen, E. M. Dewan, D. R. Moudry, F. T. Sao Sabbas, M. J. Heavner, and J. Morrill (2003), Simultaneous observations of mesospheric gravity waves and sprites generated by a midwestern thunderstorm, *J. Atmos. Sol. Terr. Phys.*, *65*, 537–550, doi:10.1016/S1364-6826(02)00328-0.

Smith, S. M., S. L. Vadas, W. J. Baggaley, G. Hernandez, and J. Baumgardner (2013), Gravity wave coupling between the mesosphere and thermosphere over New Zealand, *J. Geophys. Res. Space Physics*, *118*, 2694–2707, doi:10.1002/jgra.50263.

Smith, S. M., C. R. Martinis, J. Baumgardner, and M. Mendillo (2015), All-sky imaging of transglobal thermospheric gravity waves generated by the March 2011 Tohoku Earthquake, *J. Geophys. Res. Space Physics*, *120*, 10,992–10,999, doi:10.1002/2015JA021638.

Suppasri, A., N. Shuto, F. Imamura, S. Koshimura, E. Mas, and A. C. Yalciner (2013), Lessons learned from the 2011 Great East Japan tsunami: Performance of tsunami countermeasures, coastal buildings, and tsunami evacuation in Japan, *Pure Appl. Geophys.*, *170*(6–8), 993–1018.

Suzuki, S., K. Shiokawa, Y. Otsuka, T. Ogawa, K. Nakamura, and T. Nakamura (2007), A concentric gravity wave structure in the mesospheric airglow images, *J. Geophys. Res.*, *112*, D02102, doi:10.1029/2005JD006558.

Suzuki, S., S. L. Vadas, K. Shiokawa, Y. Otsuka, S. Kawamura, and Y. Murayama (2013), Typhoon-induced concentric airglow structures in the mesopause region, *Geophys. Res. Lett.*, *40*, 1–5, doi:10.1002/2013GL058087.

Tang, L., et al. (2012), Direct energy estimation of the 2011 Japan tsunami using deep-ocean pressure measurements, *J. Geophys. Res.*, *117*, C08008, doi:10.1029/2011JC007635.

Taylor, M. J., and H. A. Hapgood (1988), Identification of a thunderstorm as a source of short period gravity waves in the upper atmospheric nightglow emissions, *Planet. Space Sci.*, *36*, 975–985, doi:10.1016/0032-0633(88)90035-9.

Taylor, M. J., J.-M. Jahn, S. Fukao, and A. Saito (1998), Possible evidence of gravity wave coupling into the mid-latitude *F* region ionosphere during the SEEK Campaign, *Geophys. Res. Lett*, *25*, 1801–1804, doi:10.1029/97GL03448.

Tsugawa, T., Y. Otsuka, A. J. Coster, and A. Saito (2007), Medium-scale traveling ionospheric disturbances detected with dense and wide TEC maps over North America, *Geophys. Res. Lett.*, *34*, L22101, doi:10.1029/2007GL031663.

Tsugawa, T., A. Saito, Y. Otsuka, M. Nishioka, T. Maruyama, H. Kato, T. Nagatsuma, and K. T. Murata (2011), Ionospheric disturbances detected by GPS total electron content observation after the 2011 off the Pacific coast of Tohoku Earthquake, *Earth Planets Space*, *63*, 875–879, doi:10.5047/eps.2011.06.035.

Tsunoda, R. T. (2010), On seeding equatorial spread *F*: Circular gravity waves, *Geophys. Res. Lett.*, *37*, L10104, doi:10.1029/2010GL043422.

Vadas, S. L. (2007), Horizontal and vertical propagation and dissipation of gravity waves in the thermosphere from lower atmospheric and thermospheric sources, *J. Geophys. Res.*, *112*, A06305, doi:10.1029/2006JA011845.

Vadas, S. L. (2013), Compressible f-plane solutions to body forces, heatings, and coolings, and application to the primary and secondary gravity waves generated by a deep convective plume, *J. Geophys. Res. Space Physics*, *118*, 2377–2397, doi:10.1002/jgra.50163.

Vadas, S. L., and D. C. Fritts (2005), Thermospheric responses to gravity waves: Influences of increasing viscosity and thermal diffusivity, *J. Geophys. Res.*, *110*, D15103, doi:10.1029/2004JD005574.

Vadas, S. L., and D. C. Fritts (2009), Reconstruction of the gravity wave field from convective plumes via ray tracing, *Ann. Geophys.*, *27*, 147–177, doi:10.5194/angeo-27-147-2009.

Vadas, S. L., and G. Crowley (2010), Sources of the traveling ionospheric disturbances observed by the ionospheric TIDDBIT sounder near Wallops Island on 30 October 2007, *J. Geophys. Res.*, *115*, A07324, doi:10.1029/2009JA015053.

Vadas, S. L., and H.-L. Liu (2009), The generation of large-scale gravity waves and neutral winds in the thermosphere from the dissipation of convectively-generated gravity waves, *J. Geophys. Res.*, *114*, A10310, doi:10.1029/2009JA014108.

Vadas, S. L., and H.-L. Liu (2013), Numerical modeling of the large-scale neutral and plasma responses to the body forces created by the dissipation of gravity waves from 6 h of deep convection in Brazil, *J. Geophys. Res. Space Physics*, *118*, 2593–2617, doi:10.1002/jgra.50249.

Vadas, S. L., and M. J. Nicolls (2009), Temporal evolution of neutral, thermospheric winds and plasma response using PFISR measurements of gravity waves, *J. Atmos. Sol. Terr. Phys.*, *71*, 740–770, doi:10.1016/j.jastp.2009.01.011.

Vadas, S. L., J. Yue, C.-Y. She, P. A. Stamus, and A. Z. Liu (2009), A model study of the effects of winds on concentric rings of gravity waves from a convective plume near Fort Collins on 11 May 2004, *J. Geophys. Res.*, *114*, D06103, doi:10.1029/2008JD010753.

Vadas, S. L., J. Yue, and T. Nakamura (2012), Mesospheric concentric gravity waves generated by multiple convection storms over the North America Great Plain, *J. Geophys. Res.*, *117*, D07113, doi:10.1029/2011JD017025.

Vadas, S. L., H.-L. Liu, and R. S. Lieberman (2014), Numerical modeling of the global changes to the thermosphere and ionosphere from the dissipation of gravity waves from deep convection, *J. Geophys. Res. Space Physics*, *119*, 7762–7793, doi:10.1002/2014JA020280.

Vadas, S. L., J. J. Makela, M. J. Nicolls, and R. F. Milliff (2015), Excitation of gravity waves by ocean surface wave packets: Upward propagation and reconstruction of the thermospheric gravity wave field, *J. Geophys. Res. Space Physics*, *120*, 9748–9780, doi:10.1002/2015JA021430.

Walterscheid, R. L., G. Schubert, and D. G. Brinkman (2001), Small scale gravity waves in the upper mesosphere and lower thermosphere generated by deep tropical convection, *J. Geophys. Res.*, *106*, 31,825–31,832, doi:10.1029/2000JD000131.

Williams, P. J. S., et al. (1988), The generation and propagation of atmospheric gravity waves observed during the World-wide Atmospheric Gravity wave Study (WAGS), *J. Atmos. Terr. Phys.*, *50*, 323–338, doi:10.1016/0021-9169(88)90018-9.

Yeh, K. C., and C. H. Liu (1974), Acoustic gravity waves in the upper atmosphere, *Rev. Geophys.*, *12*, 193–216, doi:10.1029/RG012i002p00193.

Yue, J., S. L. Vadas, C.-Y. She, T. Nakamura, S. C. Reising, H.-L. Liu, P. Stamus, D. A. Krueger, W. Lyons, and T. Li (2009), Concentric gravity waves in the mesosphere generated by deep convective plumes in the lower atmosphere near Fort Collins, Colorado, *J. Geophys. Res.*, *114*, D06104, doi:10.1029/2008JD011244.